Cement & Concrete Composites 30 (2008) 898–906

Contents lists available at ScienceDirect

Cement & Concrete Composites

journal homepage: www.elsevier.com/locate/cemconcomp

Influence of bond properties on the tensile behaviour of Textile Reinforced Concrete

Jens Hartig *, Ulrich Häußler-Combe, Kai Schicktanz

Institute of Concrete Structures, Faculty of Civil Engineering, Technische Universität Dresden, D-01062 Dresden, Germany

ARTICLE INFO

Article history:
Received 8 November 2007
Received in revised form 18 August 2008
Accepted 30 August 2008
Available online 7 September 2008

Keywords:
Textile reinforced concrete
Non-linear analysis
Bond
Slip
Cracking

ABSTRACT

Textile Reinforced Concrete shows a complex mechanical behaviour, which arises from the heterogeneity of the cementitious matrix and the reinforcement yarn, as well as different bond conditions inside the yarn. In this contribution, a reduced two-dimensional model for simulating the uniaxial tensile behaviour of Textile Reinforced Concrete is presented. In the model, the longitudinal (loading) direction is discretised over the whole specimen length, while in the cross-sectional direction only the heterogeneity of the reinforcement is modelled by dividing the yarns into homogeneous segments arranged in a regular lattice scheme. The model also includes limited tensile strength for the matrix and the reinforcement, as well as a non-linear bond law with bond degradation between the constituents of the composite. Parametric studies are performed to show how the bond properties, e.g. the maximum bond stresses or the penetration depth of matrix in the yarns, influence the structural behaviour and the local load-bearing behaviour.

1. Introduction

Textile Reinforced Concrete (TRC) is a composite material, which has been considered as a building material for more than a decade [1]. The material offers the opportunity to construct thin structural elements for structural retrofitting and for new construction. Typically, structural elements of TRC consist of several layers of textile fabrics of multi-filament yarns made of alkali-resistant glass or carbon, which are embedded in a fine-grained concrete having aggregates with a maximum size of 1 mm. The development of the knowledge base concerning TRC is documented in [2–4] and culminated recently in a RILEM state-of-the-art report [5]. However, a number of open questions still exist. In this context, this contribution aims to demonstrate the influence of bond properties on the tensile behaviour from a mechanical point of view. To verify the calculations, experimental results of specimens reinforced with unidirectional yarns are used instead of more common bidirectional textiles.

While at the macro-scale first applicable models for the mechanical description of the structural behaviour exist [6], the behaviour at the microscopic scale, on which the macroscopic behaviour is based, is so far not sufficiently understood. In this contribution, we enhance a model on the microscopic scale, which was, from a more geometrical point of view, recently presented in [7]. It can be classified as a reduced two-dimensional model because only the longitudinal (loading) direction is discretised over the whole specimen length. Contrary to modelling strategies for steel reinforced concrete and fibre reinforced plastics, the transverse direction (which merges the directions i and j in Fig. 1) has to be discretised, because of the heterogeneity of the reinforcement and the incomplete penetration of the reinforcement with matrix. Hence, it is not appropriate to apply a homogenization method to represent the properties of the whole composite in one bar element, because matrix and reinforcement will deform differently depending on their bond and respective stiffnesses. The discretisation of the reinforcement in transverse direction is realised with a subdivision into segments, which are arranged in a regular lattice scheme (Fig. 1).

The main advancements compared to [7] are an enhanced bond description, which includes the degradation of the bond after reaching a certain maximum value of bond stress and a finer resolution of the reinforcement in the transverse direction. Thus, we are able to study the influence of a number of bond properties, as for instance the bond strength or the degree of penetration of the reinforcement with matrix, on the structural behaviour of TRC under uniaxial tensile loading. Besides simulating the global response of such structures, the model is also capable of investigating properties and effects, which are difficult or impossible to determine experimentally, such as the local stress distribution inside the material. This is essential for the understanding of the macroscopic structural behaviour, which is based on the mechanical behaviour at smaller scales.

The paper is divided into three main parts. In Section 2, the essential properties and effects of the material behaviour are described. Also in this section, the model for the simulation of the structural behaviour of textile reinforced concrete under uniaxial tensile loading is presented. In Section 3, the model is verified

* Corresponding author. Tel.: +49 351 463 333 11; fax: +49 351 463 372 79.
E-mail address: jens.hartig@tu-dresden.de (J. Hartig).

0958-9465/$ - see front matter © 2008 Elsevier Ltd. All rights reserved.
doi:10.1016/j.cemconcomp.2008.08.004

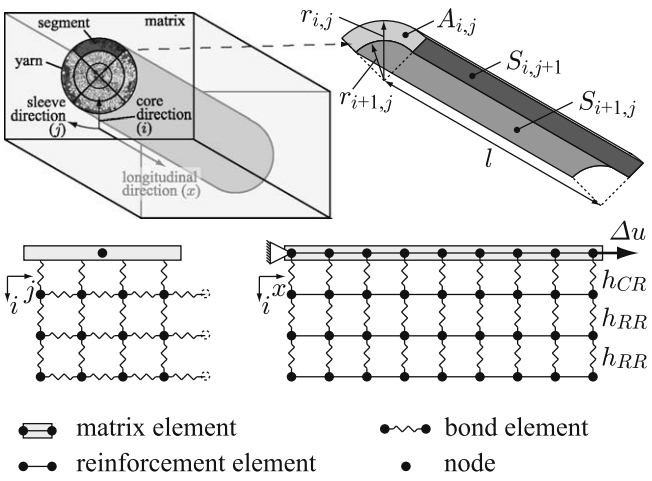

Fig. 1. Geometrical model (top) and lattice discretisation of the cross section (bottom left) and the longitudinal section (bottom right).

through comparisons with experimental results. This is followed in Section 4 by the presentation and explanation of computational results produced during parametric studies on a number of bond properties.

2. Model description

2.1. Essential properties and effects

The material behaviour of TRC is subject to a number of effects, which result from the material behaviour of the composite's components and from the interaction between the components. At first, we want to describe these effects qualitatively as we understand them currently. The matrix, a so-called fine-grained concrete, has a maximum aggregate size of 1 mm. Thus, it has properties more like a mortar than a concrete. Consequently, the matrix has a high tensile strength but a low fracture energy compared to normal concretes [8].

A reinforcement yarn typically consists of 400 up to 2000 single filaments depending on the type of the yarn, which leads to a heterogeneous structure. In tensile tests, it is observable that the filaments fail in a brittle manner [9]. In contrast, the yarns show remarkable quasi-ductility. The strength of the yarns is lower compared to the mean strength of the filaments. This can be explained by statistical effects [10] and damaging of filaments during production and processing.

Hitherto, the mechanical properties for the components of the composite were described independent of their interaction. As in every composite, the interaction between matrix and reinforcement plays a major role regarding the mechanical behaviour. A speciality of TRC compared to other composites is, besides the heterogeneous structure of the reinforcement, also the fact that the yarns are not completely penetrated with matrix. It is rather observable that only the filaments in an annular border zone of a yarn have contact with the matrix. The size of this so-called fill-in zone depends on different conditions, for example the geometry of the yarn, the after-treatment of the textile (e.g. additional polymer coating of the yarn) and the processing.

Corresponding to these two zones – with and without matrix contact – inside a yarn, two different possibilities of load transmission in a yarn exist. While in the fill-in zone loads can be transferred adhesively between the matrix and the filaments, in the inner zone of a yarn only a frictional and discontinuous load transfer at the contact areas between filaments is possible. It has to be assumed that the capacity of the adhesive bond in the fill-in zone is limited and that it is subject to degradation after reaching this limit. In the course of the bond degradation, the load transfer mechanism merges gradually from adhesion into friction. This process is irreversible and leads to remaining relative displacements between matrix and reinforcement if unloading occurs.

2.2. Implementation

2.2.1. Elements

In the following, we derive a mechanical model for the uniaxial tensile behaviour that covers the before-mentioned properties. It should be emphasised that we only consider uniaxial tensile loading on the structural level. Therefore, a one-dimensional model is basically sufficient. The model consists of two types of elements: bar elements, which represent the matrix and the reinforcement, and bond elements, which represent the matrix–filament interaction and the filament-filament interaction in the yarn, see Fig. 1.

A stiffness resulting from the cross-sectional area of each component of the composite and the Young's modulus of the respective material is assigned to the bar elements. For the bar elements representing the matrix, limited tensile strength with brittle failure is implemented, leading to cracking. For the bar elements representing the reinforcement, also brittle failure after reaching the tensile strength is assumed.

The interactions between the matrix and the reinforcement are represented by zero-thickness bond elements, which act according to bond laws h formulated as bond stress–slip relations

$$\tau = h(s) \tag{1}$$

with the bond stress τ and the slip s, which is the value of the relative displacement of the two nodes of a bond element directed in the longitudinal direction due to the one-dimensionality of the model. In order to cover a broad range of possible bond stress–slip relations, the bond laws are formulated as a set of supporting points, e.g. $(s^{ini}_{max}, \tau^{ini}_{max})$ or $(s^{ini}_{res}, \tau^{ini}_{res})$ in Fig. 2, with a suitable interpolation scheme. The interpolation between the supporting points is realised by means of the "Cubic Hermite Interpolating Polynomial Procedure" (PCHIP) approach [11]. It uses a subset of cubic polynomials, which show monotonicity and continuity in the first derivatives between consecutive intervals. This avoids, or at least reduces, numerical problems during computations on the transitions between the intervals of the bond law.

The bond law for parts of the reinforcement, which interact directly with the matrix in the fill-in zone, is shown in Fig. 2 as well as the supporting points for the interpolation. The first supporting

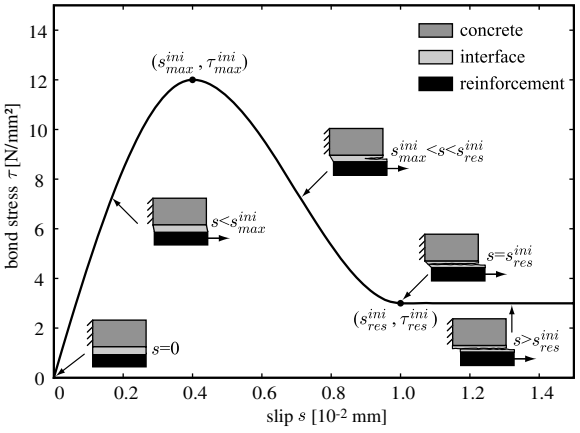

Fig. 2. Bond stress–slip relation h_{CR} for the interaction of concrete and reinforcement in the fill-in zone in the initial state.

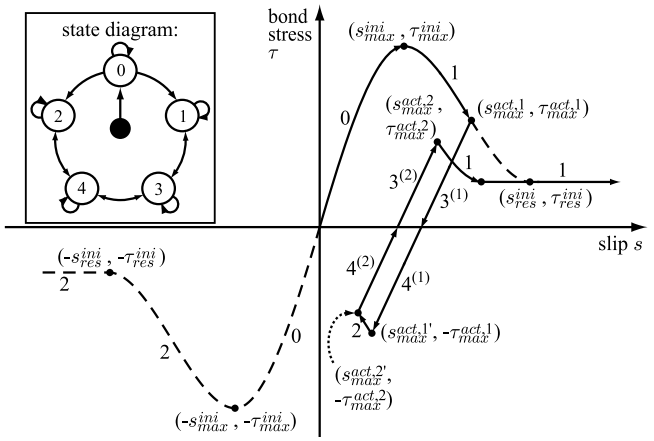

Fig. 3. Degradation algorithm in bond stress–slip relation h_{CR} exemplified with an arbitrarily chosen loading path.

point is the origin of the reference system, which is followed by a maximum value $(s^{ini}_{max}, \tau^{ini}_{max})$ according to the assumption of an initially adhesive bond. In this context, the slip s up to the value s^{ini}_{max} can be interpreted as a shear deformation of a thin interface layer between the matrix and the reinforcement. Thus, the bond stress increases with increasing slip values in this so-called state 0 according to the state diagram in Fig. 3. After this maximum point, bond degradation combined with a transition to frictional load transfer is assumed, which is finished reaching the residual point $(s^{ini}_{res}, \tau^{ini}_{res})$. After this point, purely frictional load transfer is assumed, which is implemented in the bond law with a constant value τ^{ini}_{res}. As it was mentioned in the previous section, the bond degradation is irreversible. Therefore, in state 1 of the bond stress–slip relation, see Fig. 3, an unloading path (state 3) differing from the loading path (state 1) is implemented.

It works as follows: if the absolute slip value reduces in the states 1 or 2, e.g. due to some unloading caused by local stress redistribution, the absolute value of the bond stress τ^{act}_{max} corresponding to the maximum reached slip value s^{act}_{max} is set as new maximum value. The unloading path is implemented as a linear function with a slope, which is chosen as the slope between the points (0,0) and $(s^{ini}_{max}, \tau^{ini}_{max})$. The bond stress changes according to the unloading path and the respective slip value as long as $-\tau^{act}_{max} \leqslant \tau(s) \leqslant \tau^{act}_{max}$ in the states 3 and 4, see Fig. 3. If $\tau(s)$ exceeds the value $-\tau^{act}_{max}$ in state 4, the bond law skips into state 2 with a course corresponding to state 1 but with reversed signs. Otherwise, if $\tau(s)$ exceeds τ^{act}_{max} in state 3, it skips into state 1 again. It should be noticed that the shape of the initial interpolation is maintained but the function is not reachable anymore for bond stress values $\tau(s) > \tau^{act}_{max}$ and $\tau(s) < -\tau^{act}_{max}$ respectively. The reduction of the maximum bond stress proceeds until one of the horizontal branches is reached. This approach corresponds to the concept of plasticity with a softening limit strength and progressing degradation of the material.

2.2.2. Geometry

The geometrical arrangement of the bar elements and the bond elements was introduced in principle in [7], where the reinforcement was only divided into two segments, one for the fill-in zone and one for the core zone. A similar approach is used by [12,13]. The main difference between both approaches is the connection of the reinforcement core, which is linked by [12,13] directly to the matrix, but indirectly via the fill-in zone in our approach. The indirect connection leads, in our opinion, to a more realistic description of the load distribution especially after matrix cracking. In [7], a more general description of the discretisation of the reinforcement yarn than two reinforcement segments is presented. In the following, we will briefly revise this approach.

In longitudinal direction the components of the composite are discretised in this approach as strands of bar elements with properties described in the previous section. The matrix component is discretised as a single strand of bar elements and thus it is assumed homogeneous in transverse direction. The cross-sectional area of the matrix is given by $A_{matr} = w_{matr} \cdot h_{matr}$ where w_{matr} is the width and h_{matr} is the height of the matrix or the specimen respectively. The cross-sectional area of the reinforcement is small compared to that of the matrix and is therefore neglected.

Although, we have a one-dimensional model for the strands and thus there are only degrees of freedom in longitudinal direction, the heterogeneity of the reinforcement in transverse direction is considered. This is realised with a regular segmentation of the reinforcement in radial direction i ($i \in \mathbb{N} | 1 \leqslant i \leqslant m$) and tangential direction j ($j \in \mathbb{N} | 1 \leqslant j \leqslant n$) as it is observable at the top of Fig. 1. Because in the following parametric studies only a segmentation in radial direction will be performed, the index j is equal to 1 and it will not be considered in the following derivations. Furthermore, every segment i is assumed as homogeneous with mean properties of the number of filaments, which it represents.

The cross-sectional area of a yarn A_{yarn} is approximated by the product of the mean cross-sectional area of the filaments $\bar{A}_{fil}$ and the number of filaments n_{fil} of a yarn:

$$A_{yarn} = n_{fil} \cdot \bar{A}_{fil}. \tag{2}$$

Assuming that the cross-sectional area A_{yarn} is a perfect circular area, which might underestimate the dimensions of a yarn [14], leads with the radius r to $A_{yarn} = \pi \cdot r^2$. Hence, a certain segment i has a cross-sectional area A_i of

$$A_i = \pi\left(r_i^2 - r_{i+1}^2\right), \tag{3}$$

which is an annulus. As it can be seen, r_i is the outer radius while r_{i+1} is the inner radius of the segment i. If more than one yarn is considered, it is assumed that the cross-sectional area of a segment i can be estimated by

$$A_i = n_{yarn} \cdot \pi\left(r_i^2 - r_{i+1}^2\right) \tag{4}$$

where n_{yarn} is the number of yarns. As mentioned before, the reduction of the cross-sectional area of the matrix due to reinforcement is neglected.

The interaction between the bar element strands is controlled by a bond law h as described in the previous section. To calculate bond forces resulting from the bond stresses, the estimation of bonded surface areas is necessary. Therefore, the different bond characteristics in the the fill-in zone and the core zone have to be considered. While the bonded surfaces in the fill-in zone prove to be widely continuous because of the penetration with matrix, they have to be regarded as discontinuous in the core zone due to the warping and imperfect alignment of the filaments. To solve this problem, we vary the bond laws h while we estimate the bonded surface areas according to the segmentation approach.

According to the lattice scheme, every segment interacts for $i < m$ with two adjacent segments in radial direction. For $i = m$, which means the innermost reinforcement segment, the segment interacts only with another one. Thus between two segments i and $i + 1$, the bond area is given by the arc length of the respective segment and the length l in longitudinal direction:

$$S_i = l \cdot 2\pi r_i. \tag{5}$$

If more than one yarn is considered, the bond areas can be multiplied with the number of yarns n_{yarn} as all yarns are assumed to behave equally. For one segment i, the total bond force T_i is given for $i < m$ by the sum of the bond forces of the two interfaces:

$$T_i = T_{i+1} + T_{i-1} = h(s)_{i+1} \cdot S_{i+1} + h(s)_{i-1} \cdot S_{i-1}. \quad (6)$$

For $i = m$ the bond force is given with:

$$T_i = T_{i-1}. \quad (7)$$

2.2.3. Numerical Methods

For the solution of the equations resulting from the beforementioned model, a finite element framework is chosen. The non-linear bond laws, the limited strengths of the matrix and the reinforcement lead to a highly non-linear problem. Therefore, the load is applied to the model incrementally increasing, which makes equilibrium iterations in every load step necessary. The tensile failure of the bar elements is restricted to one element per load step and after each element failure a recalculation at the same load level is performed. This prevents a simultaneous failure of a number of elements in the case of constant or nearly constant stresses in longitudinal direction and it guarantees a correct description of the load transfer between the matrix and the reinforcement in the states of crack propagation. As iteration method the Broyden–Fletcher–Goldfarb–Shanno (BFGS) approach [15,16], which is a Quasi-Newton method, in combination with line search [17] is used.

3. Model verification

3.1. Experimental results

Experimental data are used to verify the computational results. We want to limit our focus on tensile specimens for example by [14,18]. In these experiments, a sufficiently large number of yarns embedded in the matrix is available to enable multiple cracking of the matrix.

There exists a vast number of experimental results by [14,19,20,18]. Due to the availability of the original experimental data, we only concentrate on results by [14,19,20]. In Fig. 4, the geometry of a respective tensile plate specimen is shown. Typically, a reinforcement ratio in a range of about 1% up to 3% is chosen, which corresponds to a number of yarns in a range of about 50 up to 300 in the cross section. The experimental data are given as mean stress-mean strain relations where the mean stress is calculated from the measured force and the cross-sectional area of the matrix while the mean strain is the measured displacement related to the measurement length, see Fig. 4. The stress–strain relation

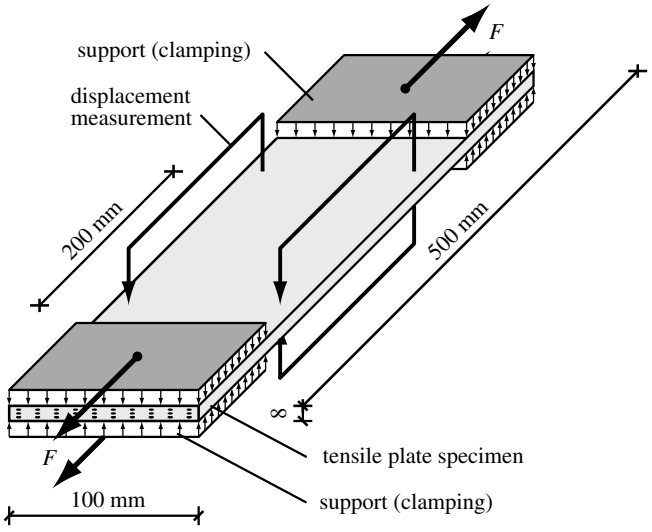

Fig. 4. Typical specimen and test setup used by [14] for tensile tests of TRC.

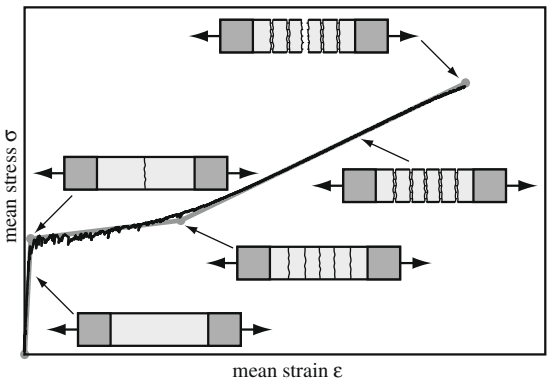

Fig. 5. Typical stress–strain relation and associated crack pattern in principle for tensile plate specimens under monotonic tensile loading.

starts, in the so-called state I, with an almost linear increase according to the Young's modulus of the matrix until the tensile strength of the matrix is reached and the matrix cracks, see Fig. 5. In the following, the reinforcement bridges the crack and because there is a sufficient amount of reinforcement available to retransmit enough forces back to the matrix, the tensile strength of the matrix will be reached again. The further cracking, in this so-called state IIa, leads to a flatter slope of the stress–strain relation compared to the uncracked state combined with a saw tooth course depending on the reinforcement ratio. When the final crack pattern is formed, the slope of the stress–strain relation becomes steeper again, which mainly results from the Young's modulus of the reinforcement. However, the matrix also participates in the load-bearing between the cracks leading to the tension stiffening effect. This state is called state IIb.

3.2. Model parameters

As a starting point for the following parametric studies, we first give an overview of the parameter values used for the model. While some of them are chosen according to experimental investigations, others have to be assumed because of a lack of corresponding experimental data. Especially concerning the bond properties, experimental investigations are rare and show high scatter. Furthermore, the bond properties depend on a large number of influences based on the production and treatment process, as for example moisture, the sizing and coating of the reinforcement or the textile processing to mention only a few. Thus, the bond properties as chosen in the following are not fixed, but serve as a basis for parametric studies.

The composition of the matrix used in the experiments, which are chosen to verify the model, is documented in [21]. The Young's modulus is determined with $28,500\text{N/mm}^2$ and the tensile strength has a value of 6.5N/mm^2. The specimen in the experiments has dimensions of 500 mm × 99.5 mm × 7.75 mm ($l_{\text{matr}} \times w_{\text{matr}} \times h_{\text{matr}}$), which results in a cross-sectional area of 771mm^2. The reinforcement was made of yarns of alkali-resistant glass with a size of 310 tex consisting of 800 filaments and it was produced by Nippon Electric Glass. The Young's modulus is given with $79,950\text{N/mm}^2$ and the tensile strength is assumed with 1357N/mm^2 according to [9]. The total cross-sectional area of the reinforcement is given by the yarn's cross-sectional area of 0.11mm^2 and a number of 134 yarns leading to 14.74mm^2, which corresponds to a reinforcement ratio of about 1.9 %. This is a typical reinforcement ratio in the center of the range performed by [14]. The reduction of the cross-sectional area of the matrix due to the reinforcement is neglected.

Furthermore, we assume that 25 % of the cross-sectional area of the reinforcement is embedded in the matrix while the other 75 % of the reinforcement in the core are not penetrated with matrix. This ratio is chosen according to values by [14] based on microscopic investigations of transparent cuts of yarns embedded in fine-grained concrete. As mentioned before, the estimation of the bond properties is associated with uncertainties. Thus, the values, which are chosen in the following, have to be considered as first estimations and have to be supported by further parametric studies. For the bond law for matrix–filament interaction h_{CR}, we assume the initial parameters given in Fig. 2. For the frictional bond law h_{RR}, we choose the same bond law except for the maximum bond stress value, which is assumed $\tau_{max}^{ini} = \tau_{res}^{ini} = 3\mathrm{N/mm^2}$.

In the Finite Element model, we use a length of 0.1 mm for the bar elements, which leads to 5000 elements per strand. This discretisation is necessary to approximate the detailed stress profiles. It should be mentioned that only the bar elements in the centre part of the model on a length of 300 mm are allowed to fail, because of reaching their tensile strength. Moreover, load transmission zones, on a length of 100 mm at both ends of the specimen, are given corresponding to the experiments, see Fig. 4. The bar elements in these zones are not allowed to fail to preserve an undisturbed load transmission from the matrix to the reinforcement. This also corresponds to experimental observations. The boundary conditions are applied to the fixed first node of the concrete segment at $x = 0$ and the prescribed displacements at the last node at $x = l$ of the concrete segment. If not otherwise stated, this configuration is used in the following parametric studies.

3.3. Influence of the reinforcement discretisation

At first, we study the influence of the reinforcement discretisation in transverse direction or the segmentation respectively. For the fill-in zone, the assumption of global load sharing between the filaments is valid, which means a uniform load distribution for all filaments. This justifies the discretisation of the fill-in zone as one sleeve segment. For the reinforcement core, local load sharing has to be assumed, which means load distribution depending on the position of the filament in the core. This calls for a finer segmentation. Therefore, a parametric study is carried out in which simulations with different numbers of core segments n_{core} are performed.

We assume that all segments have the shape of an annulus. Thus, the cross-sectional area of the sleeve segment is given by

$$A_{\mathrm{sleeve}} = n_{\mathrm{yarn}} \cdot (1-\alpha) \cdot A_{\mathrm{yarn}} \quad \text{with } 0 \leqslant \alpha \leqslant 1 \tag{8}$$

where α is the percentage of the reinforcement core on the total cross-sectional area of the reinforcement. Accordingly, the cross-sectional area of the whole reinforcement core is given with

$$A_{core} = n_{\mathrm{yarn}} \cdot \alpha \cdot A_{\mathrm{yarn}}. \tag{9}$$

It is assumed that for the core segments the condition

$$r_i - r_{i+1} = \frac{r_{core}}{n_{core}} = \frac{\sqrt{\frac{\alpha \cdot A_{\mathrm{yarn}}}{\pi}}}{n_{core}} = \mathrm{const} \tag{10}$$

applies where r_{core} is the radius of the total core. This condition is chosen because it seems to represent the failure behaviour more realistic as for example a discretisation with equal cross-sectional areas. In the numerical studies, which are presented here, only a segmentation of the reinforcement in radial direction is performed. While this is appropriate for a deterministic approach, stochastic variations of the filament strength would require an additional segmentation in tangential direction. This has to be treated in further investigations. Thus, for a core segment i the cross-sectional area is given according to Eq. (4) by

$$A_{core,i} = n_{\mathrm{yarn}} \cdot \alpha \cdot \pi\left(r_i^2 - r_{i+1}^2\right). \tag{11}$$

Furthermore, the respective bond areas S_i are given according to Eq. (5).

In Fig. 6, the stress–strain relations for cases of 1, 10 and 25 core segments as well as experimental stress–strain relations with a corresponding reinforcement ratio are shown. It is observable that the macroscopic experimental behaviour, which shows only few scatter, is essentially reproduced by the model. However, three deficiencies exist.

The first deficiency is the number of the calculated cracks, which is too small compared to the experiments. Supposedly, the main reason for this effect is the neglect of the post-cracking behaviour of the matrix with a crack energy and transmission of softening tensile stresses after the tensile strength is reached. Neglecting this effect while only relying on the load retransmission from the bonded reinforcement underestimates the tensile stress in the matrix and overestimates the crack width.

A second deficiency is given with several plateaus of matrix cracks in the computational results, before the final cracking state is reached. This can be explained by the deterministic modelling of the tensile strength of the matrix, which leads to the development of primary cracks with constant crack spacing. In the process of increasing loads, secondary cracks develop at the midpoint of a crack spacing leading to further crack plateaus. A stochastic modelling of the tensile strength of the matrix would lead to a less regular crack distribution but a continuous state of crack development.

In this context, it has to be noticed that the crack plateaus also differ for different segmentations, see Fig. 6. This effect can be explained with the normal stress distributions of the reinforcement segments in the longitudinal direction in Fig. 7 where the peaks in the reinforcement stresses correspond to a zero stress in the matrix indicating a matrix crack. As it can be seen in the Figs. 7a and 7b, the activated length of the reinforcement segments becomes larger towards the innermost segment. This effect is amplified with an increasing number of segments and is connected with different stress distributions. This also leads to a different development of cracks in the matrix and to different final crack patterns, see Figs. 7c and 7d. Regarding the normal stress distribution in longitudinal direction, it can be observed in Fig. 7d that the highest reinforcement stress occurs at the sleeve segment in a matrix crack. Vice versa, the core segments have higher normal stresses compared to the sleeve segment in the uncracked matrix parts. Moreover, the stress amplitudes become smaller from the sleeve segment towards the innermost core segment.

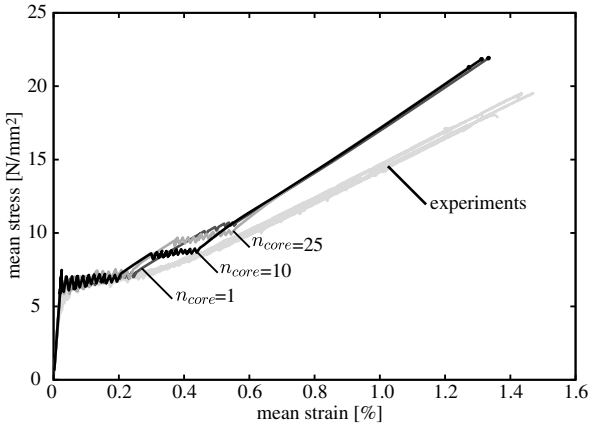

Fig. 6. Stress–strain relations for different numbers of core segments and respective experimental data.

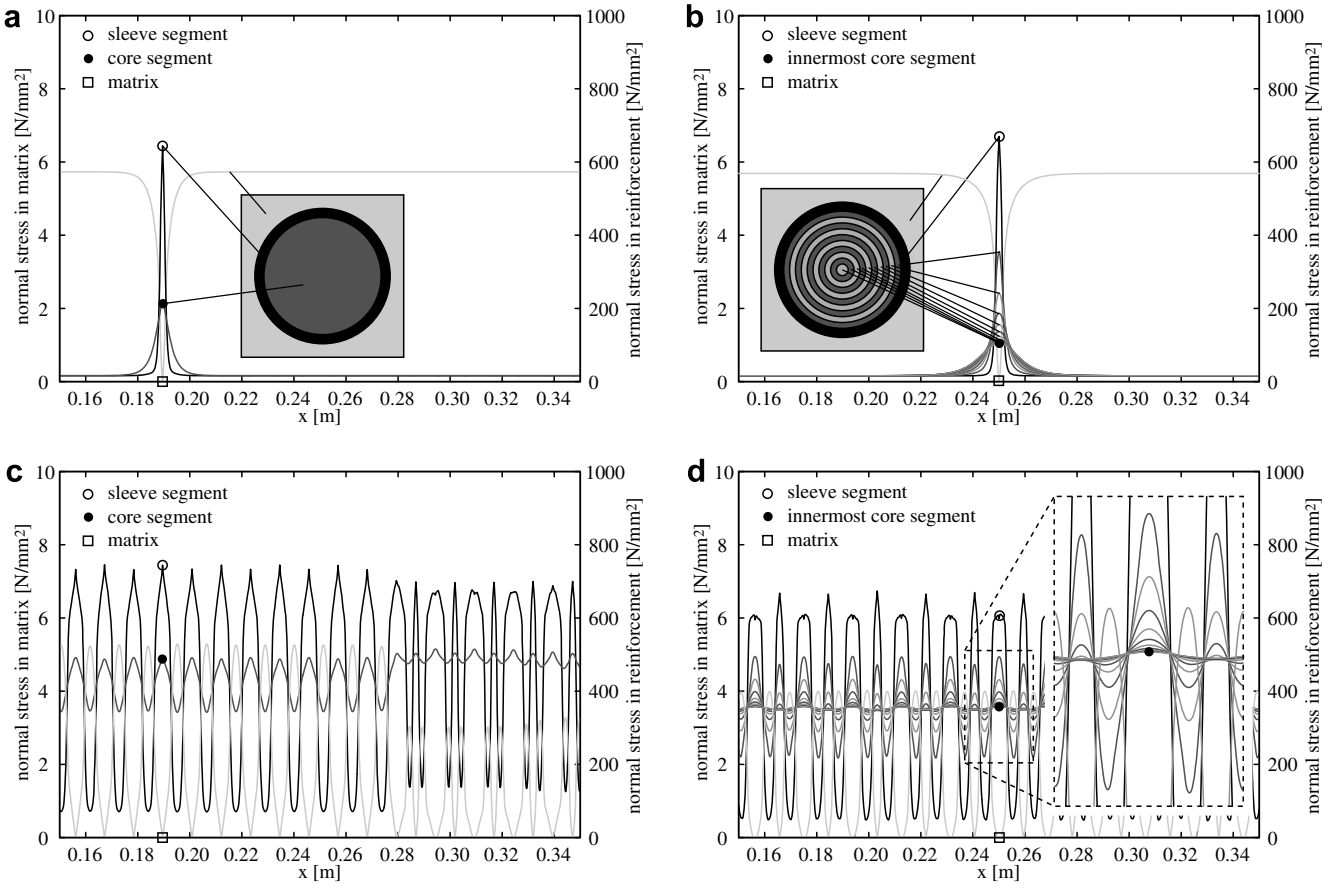

Fig. 7. Normal stresses along the longitudinal axis in the centre part of the model with different reinforcement discretisations: (a) First matrix crack, one core segment; (b) First matrix crack, ten core segments; (c) Final crack pattern, one core segment; (d) Final crack pattern, ten core segments.

The third deficiency concerns the slope of the stress–strain relation in state IIb, which is steeper compared to the experimental results, see Fig. 6. An explanation is given by [14], based on the model by [22], with the failure of the filaments in the fill-in zone simultaneously with matrix cracking. However, values of about 15 up to 25 % of failed filaments, seem to be unrealistic. Simulations show that a simultaneous failure of the filaments in the fill-in zone and the matrix leads to a strongly reduced number of cracks [23]. The reason is that less load can be retransmitted from the reinforcement to the concrete because of the strongly reduced bond in case of a failed sleeve segment.

A more appropriate explanation for the deficiency of the slope in state IIb can be given with the combination of the post-cracking behaviour of the matrix and the successive failure of the reinforcement at higher load levels. If a matrix crack occurs in state IIa, the matrix undergoes a gradual softening, which also reaches state IIb. This leads to a slower increase of the relative displacements between the matrix and the reinforcement and thus to a slower activation of the reinforcement by bond. As a consequence, the total stiffness of the specimen gradually converges towards the stiffness of the reinforcement. This stiffening is counteracted by the gradual degradation of the reinforcement caused by the failure of single filaments due to a stochastic distribution of their tensile strengths. The superposition of both effects leads to a lower slope of the stress–strain relation in state IIb. Moreover, it was shown by [24] based on enhanced fibre bundle models by [10] that usually the failure of about 10% up to 20% of the filaments of a yarn is sufficient for the failure of the whole yarn. This could explain why there is no pronounced decrease of the slope in state IIb but a sudden failure. Detailed investigations including the post-cracking behaviour of the matrix and the successive failure of the reinforcement exceed the scope of this contribution, which concentrates on the bond properties, and has to be treated in further investigations.

In Fig. 8, the evolution of the normal stresses in the sleeve segment, the innermost and the outermost core segment at the first concrete crack are shown for different discretisations of the reinforcement core. It is observable that the normal stresses of the sleeve segment increase slightly with an increasing number of core

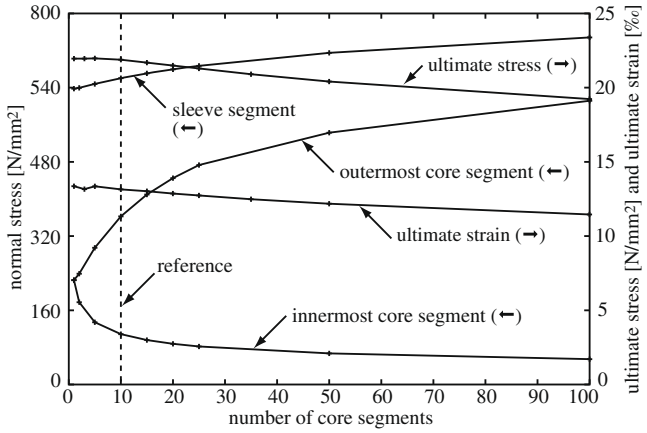

Fig. 8. Ultimate mean stresses, ultimate mean strains and normal stress at the first matrix crack in the sleeve segment, the outermost and the innermost core segment with different numbers of core segments n_{core}. The arrows in parentheses indicate the scale to be used for each curve.

segments. Simultaneously, the normal stresses in the outermost core segment increase stronger while the normal stresses in the innermost core segment decrease with increasing numbers of core segments. Regarding the ultimate stresses and strains, which are shown in Fig. 8, a slight decrease of both the ultimate mean stresses and mean strains with an increasing number of core segments is observable. This is caused by the earlier failure of the sleeve segment as the tensile stresses in the sleeve segment increase with increasing numbers of core elements, see Fig. 8.

For the following parametric studies, a number of core segments has to be chosen. Because of the strongly increasing computation time with increasing numbers of elements, the number of core segments has to be limited. Therefore, a model with one sleeve segment and ten core segments is chosen for the following parametric studies. In the following visualizations of the computational results, this configuration is marked as the reference case with a dashed line. This should facilitate the comparison between the results of the parametric studies.

4. Parametric studies

4.1. Influence of the frictional load transfer in the reinforcement core

In this section, we study the influence of the bond stress of the frictional bond law h_{RR} in the reinforcement core on the structural behaviour. Therefore, we use the model with one sleeve segment, which has a cross-sectional area of 25 % of the total cross-sectional area of the reinforcement and ten core segments leading to a value of $\alpha = 0.75$. The cross-sectional areas of the core segments can be calculated according to the Eqs. (9)–(11) and the bond areas according to Eq. (5).

In Fig. 9, the normal stresses at the first matrix crack in the sleeve segment, the innermost and outermost core segment are plotted for bond stress values $\tau^{ini}_{max} = \tau^{ini}_{res}$ of the bond law h_{RR} in a range of 0.1N/mm² up to 20N/mm². Experimental investigations indicate values of about 1N/mm². It is observable that with increasing values of the frictional bond stress in the reinforcement core the normal stress in the sleeve segment decreases while the normal stress in the innermost core segment increases. The normal stress in the outermost core segment also increases strongly with increasing values of the frictional bond stress in the core and converges towards a value of about 400N/mm². With higher values of the frictional bond stress, the values of the normal stresses adjust to homogeneity, because the load transfer changes from a more local to a more global load sharing.

Regarding the ultimate mean stresses and mean strains, it can be concluded that larger values of the frictional bond stress than 3—5N/mm² do not improve the structural performance significantly. In Fig. 9, it can be seen that up to this threshold the ultimate mean stresses and mean strains strongly increase. With larger values of the frictional bond stress these values only increase slightly. It is also observable that the course of the strains is not as smooth as that of the stresses. This can be explained by different matrix crack distributions in every simulation leading to different displacements and finally to a different mean strain.

4.2. Influence of the size of the reinforcement core

In the previous section, it was shown that the participation of the reinforcement core is important to reach a high ultimate stress. Besides improving the bond properties inside the yarns with impregnation, it is also possible to improve the penetration of the reinforcement with matrix. Thus, we study the influence of this penetration in the following. Therefore, we use again a model with one sleeve segment connected to the matrix with the bond law for matrix–filament interaction h_{CR} and ten core segments connected with the frictional bond law h_{RR} respectively with the parameters defined in Section 3.2. For the parametric study, we only vary the total cross-sectional area of the reinforcement core by the value α, see Eqs. (8)–(11).

In Fig. 10, again the normal stresses of the sleeve segment, the outermost and the innermost core segment at the first matrix crack are shown. It is observable that the innermost core segment is almost not influenced by the variation of the cross-sectional area of the reinforcement core. In contrast, the normal stress in the outermost core segment increases from about 260N/mm² at $\alpha = 0.05$ to a normal stress of about 440N/mm² at $\alpha = 0.95$. This tendency is stronger for the sleeve segment where the normal stress increases from about 350N/mm² at $\alpha = 0.05$ to a value of about 1400N/mm² at $\alpha = 0.95$. The latter normal stress value is higher than the tensile strength of the reinforcement. Thus, the sleeve segment fails simultaneously with the matrix cracks in this case. It can be seen that the differences in the normal stresses between the sleeve segment and the core segments become larger for increasing values of α. This also encourages the early failure of the respective parts of the reinforcement with the highest normal stresses.

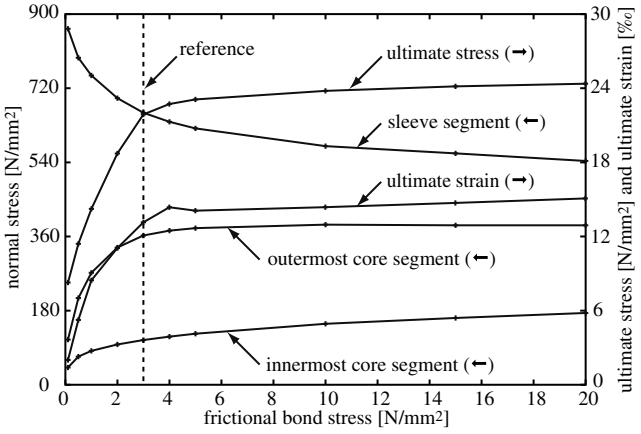

Fig. 9. Ultimate mean stresses, ultimate mean strains and normal stress at the first matrix crack in the sleeve segment, the outermost and the innermost core segment with different values of the frictional bond stress in the bond law h_{RR} in the reinforcement core. The arrows in parentheses indicate the scale to be used for each curve.

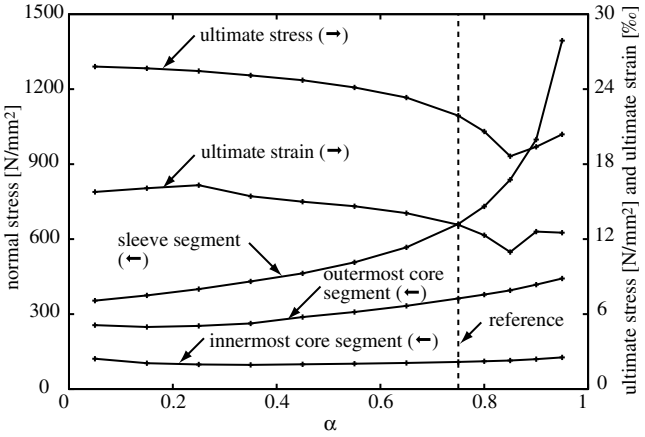

Fig. 10. Ultimate mean stresses, ultimate mean strains and normal stress at the first matrix crack in the sleeve segment, the outermost and the innermost core segment with different percentages α of the core cross-sectional area. The arrows in parentheses indicate the scale to be used for each curve.

Concerning the ultimate load, it is generally observable that a decreasing amount of reinforcement embedded in the matrix, which corresponds to increasing values of α, leads to decreasing ultimate loads, see Fig. 10. However, the minimum of the simulated ultimate load does not correspond to the lowest amount of reinforcement embedded in the matrix. It is rather observable that there is a minimum near the value $\alpha = 0.85$. With larger values of α an increase of the ultimate load is observable. This can be explained in the following way: with increasing values of α, the cross-sectional area of the sleeve segments becomes smaller, which leads to increasing normal stresses in the sleeve segment at the matrix cracks. When the sleeve segment fails, because of the cracking of the matrix, the core segments are not able to carry the additional loads and consequently they fail too in a certain range of α. With larger values than $\alpha = 0.85$, the core segments are able to bear the additional loads without failing and thus slightly larger ultimate mean stresses and mean strains can be reached. A value of $\alpha = 0.85$ corresponds well to the before-mentioned observations presented in [24]. Furthermore, a lower number of matrix cracks is observable for values $\alpha > 0.85$.

4.3. Influence of the maximum adhesional bond stress

Finally, we study the influence of the maximum bond stress τ^{ini}_{max} of the bond law between the matrix and the sleeve segment h_{CR} to show the effect of a bond improvement in the fill-in zone. Again, the model configuration of Section 4.1 is used, but the frictional bond stress is kept constant at a value $\tau_{res} = 3\text{N/mm}^2$.

In Fig. 11, the normal stresses at the first matrix crack in the sleeve segment as well as the outermost and innermost core segments for maximum adhesional bond stress values in a range of 3 up to 100N/mm^2 are shown. The normal stresses in the sleeve segment increase with increasing values τ^{ini}_{max} and converge towards a constant value. It can also be seen that for 100N/mm^2 the normal stress has almost reached the tensile strength of the reinforcement, which represents the upper limit for the possible normal stress. Regarding the outermost core segment, it can be noticed that the normal stresses firstly increase up to a value of about 365N/mm^2 with $\tau^{ini}_{max} \approx 10\text{N/mm}^2$. With higher values of τ^{ini}_{max} the normal stresses decrease to a value of about 200N/mm^2 with $\tau^{ini}_{max} = 100\text{N/mm}^2$. This can be explained as follows. In case of smaller values than $\tau^{ini}_{max} = 10\text{N/mm}^2$, the slip between the matrix and the sleeve segment is relatively large, which leads to a large activated bond length with higher bond stresses. This leads also to relatively high relative displacements to and between the cores segments, which become generally smaller towards the innermost core segment. In case of larger values than $\tau^{ini}_{max} = 10\text{N/mm}^2$, the activated bond length between matrix and sleeve segment becomes smaller. Thus, there is also a smaller length with relative displacements between the sleeve segment and the outermost core segment, which leads to a smaller amount of load transmitted to the core and to smaller normal stresses. The innermost core segment is less effected by the change of the maximum bond stress τ^{ini}_{max} between the matrix and the sleeve segment because the influence of the matrix cracks and the respective relative displacements between the reinforcement segments decreases towards the innermost core segment. This leads to decreasing normal stresses in the innermost core segment with increasing values τ^{ini}_{max} depending on the normal stresses in the sleeve segment.

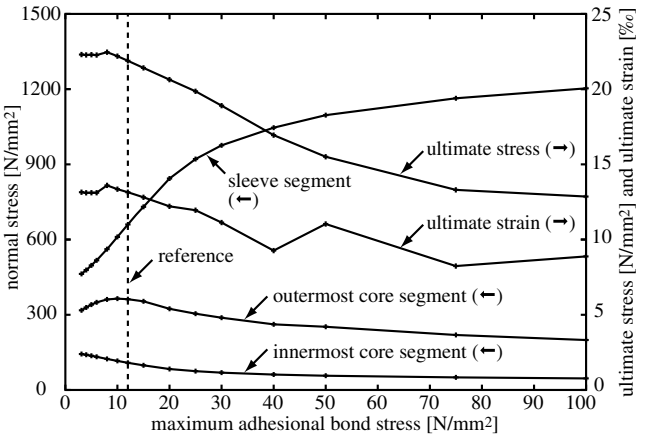

Fig. 11. Ultimate mean stresses, ultimate mean strains and normal stress at the first matrix crack in the sleeve segment, the outermost and the innermost core segment with different maximum bond stress values τ^{ini}_{max} between matrix and sleeve segment. The arrows in parentheses indicate the scale to be used for each curve.

Concerning the ultimate stresses and strains, it can be seen in Fig. 11 that up to a value of $\tau^{ini}_{max} = 10\text{N/mm}^2$ no significant change of the ultimate stresses and strains occurs. Afterwards, the ultimate stresses and strains decrease with increasing values of τ^{ini}_{max}, which can be explained again by increasing stresses at the matrix cracks because of the stronger bond. Thus, the tensile strength of the sleeve segments is reached earlier and the load is redistributed to the core segments, which cannot bear the additional loads and fail too. Hence, a too strong bond between the matrix and the filaments in the fill-in zone lead to large differences in the stresses of the reinforcement segments and to a decrease of the ultimate load.

5. Conclusions

The influence of several bond properties on the tensile behaviour of Textile Reinforced Concrete has been investigated by means of parametric studies. It was discussed how these bond properties determine the stress distribution as well as the ultimate mean stresses and mean strains of uniaxial tensile specimens.

From a macroscopic point of view, a high ultimate load is generally desired. The parametric studies showed that this requirement is always met if there is a balanced stress distribution between the sleeve zone and the core zone of the reinforcement. This means a higher difference of the normal stresses between the sleeve zone and the core zone causes earlier failure of the whole structure. With a parametric study on the frictional bond stress in the reinforcement core, it was shown that a relatively small value of the frictional bond stress can strongly improve the ultimate stresses and strains of the structure. The reason is a relatively balanced stress distribution in the reinforcement where the reinforcement sleeve is always more highly loaded than the core region of the reinforcement. Another result was that the ultimate stress level cannot be further substantially improved even with large bond stress values between the core segments. Essentially the same result was observed with the variation of the size of the reinforcement core where the highest ultimate stresses were reached with small cross-sectional areas of the reinforcement core. In a further parametric study, the maximum bond stress between the matrix and the sleeve segment was varied. These simulations showed that with an increasing bond strength between the matrix and the filaments in the fill-in zone, decreasing ultimate mean stresses and mean strains have to be expected under certain conditions. The reason for this behaviour is that the filaments in the fill-in zone are more highly loaded at the matrix cracks and fail earlier, while the reinforcement core is not able to bear the additional loads after cracking due to the unbalanced load distribution.

The presented results are primarily qualitative. It should be noticed that the values of the parameters of the bond law are chosen according to assumed bond areas, which underestimate realistic values [14]. Thus, they cannot be compared directly with

experimental values, which on the other hand show high scatter. It should also be mentioned that the tensile strengths are modelled deterministically. A stochastic modelling of the reinforcement tensile strengths could lead to improved results. However, this increases the computational costs and has to be considered in further investigations.

Acknowledgement

The authors gratefully acknowledge the financial support of this research from Deutsche Forschungsgemeinschaft DFG (German Research Foundation) within the Sonderforschungsbereich 528 (Collaborative Research Center) "Textile Reinforcement for Structural Strengthening and Retrofitting" at Technische Universität Dresden as well as their colleagues for providing the experimental data.

References

[1] Curbach M et al. Sachstandbericht zum Einsatz von Textilien im Massivbau (DAfStb Heft 488). Berlin: Beuth; 1998.
[2] Hegger J, editor. Textilbeton – 1. Fachkolloquium der Sonderforschungsbereiche 528 und 532. Aachen: RWTH Aachen; 2001.
[3] Curbach M, editor. Textile reinforced structures – proceedings of the 2nd colloquium in textile reinforced structures (CTRS2). Dresden: Technische Universität Dresden; 2003.
[4] Hegger J, Brameshuber W, Will N, editors. Textile reinforced concrete – proceedings of the 1st international RILEM symposium (RILEM PRO 50). Bagneux: RILEM Publications S.A.R.L., 2006.
[5] Brameshuber W, editor. State-of-the-art report of RILEM technical committee 201 TRC: textile reinforced concrete (RILEM Report 36). Bagneux: RILEM Publications S.A.R.L., 2006.
[6] Richter M, Zastrau BW. On the nonlinear elastic properties of textile reinforced concrete under tensile loading including damage and cracking. Mater Sci Eng A 2006;422:278–84.
[7] Häußler-Combe U, Hartig J. Bond and failure mechanisms of textile reinforced concrete (TRC) under uniaxial tensile loading. Cement Concr Compos 2007;29(4):279–89.
[8] Brockmann T. Mechanical and fracture mechanical properties of fine grained concrete for textile reinforced composites. PhD thesis. Aachen, RWTH Aachen, 2006.
[9] Abdkader A. Charakterisierung und Modellierung der Eigenschaften von AR-Glasfilamentgarnen für die Betonbewehrung. PhD thesis. Dresden, Technische Universität Dresden, 2004.
[10] Daniels HE. The statistical theory of the strength of bundles of threads I. Proc Roy Soc London 1944;A183:405–35.
[11] Fritsch F, Carlson R. Monotone piecewise cubic interpolation. SIAM J Numer Anal 1980;17(2):238–46.
[12] Hegger J, Will N, Bruckermann O, Voss S. Load-bearing behaviour and simulation of textile reinforced concrete. Mater Struct 2006;39:765–76.
[13] Bruckermann O. Zur Modellierung des Zugtragverhaltens von textilbewehrtem Beton. PhD thesis. Aachen, RWTH Aachen, 2007.
[14] Jesse F. Load bearing behaviour of filament yarns in a cementitious matrix (in German), PhD thesis. Dresden, Technische Universität Dresden, 2004.
[15] Matthies H, Strang G. The solution of non-linear finite element equations. Int J Numer Methods Eng 1979;14:1613–26.
[16] Nocedal J, Wright SJ. Numerical optimization. New York: Springer; 1999.
[17] Bathe KJ. Finite element procedures. Englewood Cliffs: Prentice-Hall; 1996.
[18] Molter M. Zum Tragverhalten von textilbewehrtem Beton. PhD thesis. Aachen, RWTH Aachen, 2005.
[19] Jesse F, Ortlepp R, Curbach M. Tensile stress–strain behaviour of textile reinforced concrete. In: Towards a better built environment – innovation, sustainability, information technology (book of abstracts), vol. 86 of IABSE report. Melbourne: International Association for Bridge and Structural Engineering; 2002. p. 376–7.
[20] Jesse F, Curbach M. Strength of continuous AR-Glass fibre reinforcement of cementitious composites. In: Naaman AE, Reinhardt HW, editors. High performance fiber reinforced cement composites (HPFRCC4). Ann Arbor: RILEM; 2003. p. 337–48.
[21] Curbach M, Jesse F. Dehnkörper aus textilbewehrtem Beton – Phänomene, Deutung, Schlußfolgerungen. In: Hegger J, editor. Textilbeton – 1. Fachkolloquium der Sonderforschungsbereiche 528 und 532. Aachen: RWTH Aachen; 2001. p. 125–36.
[22] Ohno S, Hannant DJ. Modeling the stress–strain response of continuous fiber reinforced cement composites. ACI Mater J 1994;91(3):306–12.
[23] Hartig J, Häußler-Combe U, Schicktanz K. Modelling the uniaxial load-bearing behaviour of textile reinforced concrete with a lattice approach including damage (Paper No. 17-2). In: Triantafillou T, editor. Proceedings of the 8th international symposium on fiber-reinforced polymer reinforcement for concrete structures (CD of full papers). Patras: University of Patras; 2007.
[24] Curbach M, Schicktanz K, Jesse F, Hartig J. Stochastische Eigenschaften der Zugfestigkeit freier und zementös eingebetteter Filamentbündel aus AR-Glas. In: Ruge P, Graf W, editors. 10. Dresdner Baustatik-Seminar, Neue Bauweisen – Trends in Statik und Dynamik. Dresden: Technische Universität Dresden; 2006. p. 91–100.